2026 IEEE/SICE International Symposium on System Integration (SII)
January 11-14, 2026. Cancún, México

Parameter Design Aimed at Improving the Practicality of the Multiple Virtual Dynamics-based Force Control

Mikihiro Kanekiyo, Hikaru Arita, Kazuto Nakashima, and Kenji Tahara

Abstract— **Contact task execution in unknown environments is fundamental to robotic applications, requiring three essential functions: accurate position tracking, safe contact establishment, and achievement of desired contact force. In our previous work, the Multiple Virtual Dynamics-based Force Control (MVDFC) was proposed. This method seamlessly integrates these three functions; however, several challenges remain when considering practical force control. The first challenge is that time delays in the force sensor can destabilize the control system. The second challenge is that loss of contact with the environment during a force control task can result in acceleration of robot and collisions with the environment. These two challenges are commonly encountered in various force control methods. Here, a key feature of MVDFC is its flexibility, allowing the motion of virtual objects in each virtual dynamics to be independently designed. Therefore, by leveraging this flexibility, it is possible to overcome the two challenges without compromising the three functions. This study proposes a direction for parameter design to address the above issues, and its effectiveness is demonstrated through both simulations and experiments.**

I. INTRODUCTION

In industrial robot applications, physical interaction with the environment is crucial. For example, in tasks such as polishing and deburring, the contact force should be directly controlled to achieve the desired force. To perform such tasks, the following three functions are required: the function to accurately track trajectories in mid-air, the function to safely make contact with unknown environments, and the function to accurately achieve the desired contact force under unknown environments. Here, the desired contact force can be achieved only after the former two functions are realized, and a smooth transition to force control after contact is desirable. Therefore, achieving practical contact force control requires seamless integration of all three functions.

As a force control method that integrates these three functions, Kanekiyo *et al*. proposed the Multiple Virtual Dynamics-based Force Control (MVDFC) [1]. This force control method has a three-layer structure, among which the lower two layers correspond to the series admittance-impedance control proposed by Fujiki and Tahara [2], which combines admittance control [3] and impedance control [4] in series. In this method, both accurate position tracking performance and safe contact with unknown environments, especially the suppression of oscillatory responses that tend to occur when contacting stiff environments that is characteristic of admittance control [5], [6], can be achieved by setting the parameters to make the desired impedance hard and desired admittance soft. Namely, impedance control is designed with an emphasis on tracking performance, while admittance control is designed with an emphasis on stability when contact.

Furthermore, the 3rd layer is a virtual dynamics layer designed to achieve the desired contact force. This layer incorporates two key ideas from the Multiple Virtual Dynamics-based Control (MVDC) framework [7], which was generalized by Arita *et al*. in a more universal method by focusing on the structure of connecting admittance control and impedance control in series, as originally proposed by Fujiki and Tahara [2]. The first idea is the addition of more virtual dynamics layers to create a three-layer, four-layer, or even more complex structure, not only a two-layer structure of admittance control and impedance control. The second idea is the concept of a virtual force, which treats various types of information, such as sensor outputs, as a type of force. This concept allows admittance control to be used to control the response of the virtual object to various types of information. These two ideas make it possible to design the motion of a virtual object in each virtual dynamics layer based on its respective virtual force, enabling smooth transitions between the functions of each layer. By employing the first idea of MVDC framework, Kanekiyo *et al*. added a 3rd virtual dynamics layer to seamlessly transition to force control from the series admittance-impedance control without switching the controller. Furthermore, according to the second idea of MVDC framework, a pre-designed virtual force is used as input in this layer to output the motion of a virtual object that achieves the desired contact force. In this way, the method proposed by Kanekiyo *et al*. achieves the desired contact force without compromising the advantages of Fujiki *et al*.'s method, seamlessly integrating the three functions required for the tasks involving physical interaction.

However, when considering the practical implementation of force control, there are several challenges. The first challenge is that time delays of force sensor can make the control system unstable [8], [9]. It is well known that force sensors typically exhibit time delays, and because their measurements often contain significant noise, applying filtering to reduce the noise further increases the time delay [10]. These characteristics of force sensors can degrade the responsiveness of force control and potentially affect the accuracy and stability of the control system.

The second challenge is that when contact with the environment is lost during a force control task, the end-effector may unintentionally accelerate in the direction of the force

This work was partially supported by JSPS KAKENHI Grant Number JP24H00726. The authors are with Department of Mechanical Engineering, Kyushu University, Fukuoka 819-0395, JAPAN (e-mail : kanekiyo@hcr.mech.kyushu-u.ac.jp; [arita, kazuto, tahara]@ieee.org).

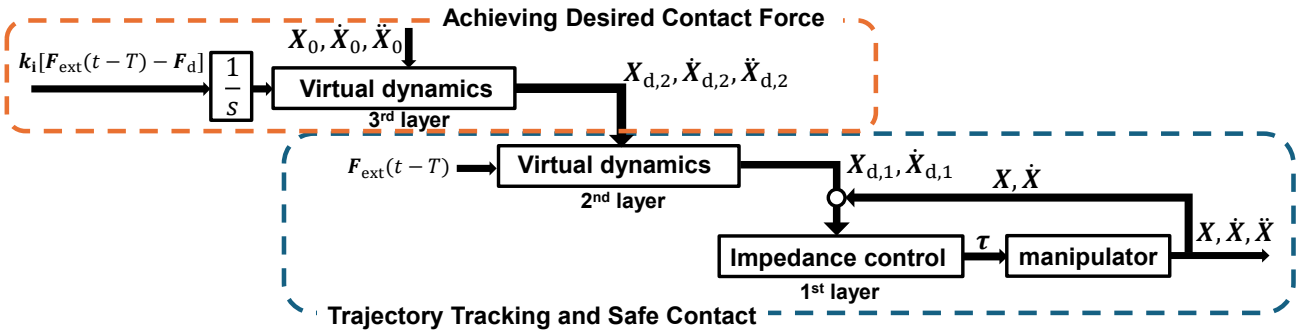

Fig. 1. Block diagram of the Multiple Virtual Dynamics-based Force Control(MVDFC). The unique point is that the position output of the 3rd virtual dynamics layer serves as the equilibrium point of the series admittance-impedance control.

control, which can lead to an undesirable collision with the environment [11], [12], [13]. In practical force control tasks such as polishing or deburring, the end-effector applies force to the contact surface and moves while maintaining contact. However, it is difficult for the robot to accurately know the shape or position of the surface of environment [14]. Therefore, the loss of contact between the end-effector and the environment is likely to occur. It is common to immediately perform an emergency stop of the robot when contact is lost due to safety concerns; however this approach often requires significant time for restarting and recovery [13], [15]. Therefore, when contact with the environment is lost, it is necessary for the robot to adjust its motion to prevent an undesirable collision, and then quickly resume the task. However, transitioning instantly from force control to such motion requires switching in the controller, which is challenging and may result in unstable robot behavior, causing dangerous situations.

These two challenges are commonly encountered in various force control methods. Here, a key characteristic of MVDFC, it offers the flexibility to independently and freely design the motion of virtual objects in each virtual dynamics. While MVDFC realizes the three functions as mentioned, there remains flexibility in the design of its parameters. Therefore, by leveraging this flexibility and appropriately designing the parameters, there is potential to address the two challenges without compromising the previously achieved three functions. For the first issue, it has been proven that stable control can be achieved by increasing the damping gain in admittance and impedance control [8]. In general, increasing the damping value in the input to the robot may lead to instability in the control system due to discretization noise in velocity feedback. On the other hand, in the case of MVDFC, the damping value is defined within the virtual dynamics and velocity feedback of the manipulator is not used in virtual dynamics. Therefore, it is considered possible to achieve stable control against sensor time delays without causing such instability. For the second issue, the motion of the virtual object influences the actual motion of the robot in MVDFC. Moreover, changing the viscosity value changes the convergence speed of the virtual object in the virtual dynamics. Therefore, by designing the viscosity separately for each virtual dynamics, it is considered possible to adjust the convergence speed of the virtual object after contact loss and control the robot's motion without switching the controller. The contributions of this paper are as follows.

- By adjusting the parameter in the virtual dynamics, it is possible to improve stability against force sensor time delays without causing control system instability due to discretization noise in velocity feedback.
- By independently designing the parameters of each virtual dynamics, the motion of the robot after loss of contact with the environment can be controlled without controller switching.

Since these can be realized solely by modifying parameters, implementation is simplified, which in turn contributes to enhancing the practical applicability of MVDFC. The above two contributions and parameter design direction are demonstrated through simulations using a two-link manipulator and experiments using an actual manipulator.

II. Multiple Virtual Dynamics-based Force Control

The force controller proposed by Kanekiyo *et al.* is intended for implementation in multiple-DOF manipulators. Therefore, we explain the method by representing the end-effector coordinates of a manipulator as $\boldsymbol{X} \in \mathbb{R}^n$ and the generalized joint coordinates as $\boldsymbol{q} \in \mathbb{R}^m$. A block diagram of the force controller is shown in Fig. 1. According to Fig. 1, the controller has a three-layer structure. The 1st and 2nd layers correspond to series admittance-impedance control [2], whereas the 3rd layer has the function of achieving the desired contact force [1]. In the following, the admittance control layer in the series admittance–impedance control is referred to as virtual dynamics layer. The equation of virtual dynamics for the 2nd layer is given as follows:

$$\begin{aligned} \boldsymbol{M}_{\mathrm{da},1}(\ddot{\boldsymbol{X}}_{\mathrm{d},1}-\ddot{\boldsymbol{X}}_{\mathrm{d},2})+\boldsymbol{D}_{\mathrm{da},1}(\dot{\boldsymbol{X}}_{\mathrm{d},1}-\dot{\boldsymbol{X}}_{\mathrm{d},2}) \\ +\boldsymbol{K}_{\mathrm{da},1}(\boldsymbol{X}_{\mathrm{d},1}-\boldsymbol{X}_{\mathrm{d},2})=\boldsymbol{F}_{\mathrm{ext}}(t-T), \end{aligned} \tag{1}$$

where $\boldsymbol{X}_{\mathrm{d},1}$ denotes the position of the virtual object; $\boldsymbol{X}_{\mathrm{d},2}$ denotes the desired position for the 2nd layer; and $\boldsymbol{M}_{\mathrm{da},1}$, $\boldsymbol{D}_{\mathrm{da},1}$, and $\boldsymbol{K}_{\mathrm{da},1}$ denote the nominal desired inertia, viscosity, and stiffness matrices, respectively. In addition, $\boldsymbol{F}_{\mathrm{ext}}$ denotes the external force applied to the end-effector of the

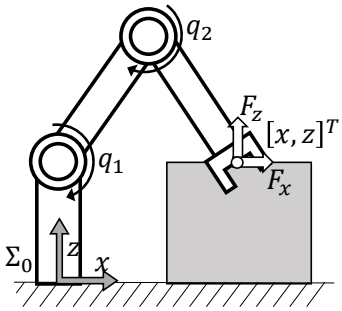

Fig. 2. 2-DOF manipulator model on a 2D plane. The end-effector is in contact with the environment, and an external force is applied.

manipulator and T denotes the dead time of force sensor. Next, the torque input to the manipulator in impedance control $\boldsymbol{\tau}$ is given as follows:

$$\boldsymbol{\tau} = -\boldsymbol{J}^\top\{\boldsymbol{D}_{\mathrm{di}}(\dot{\boldsymbol{X}} - \dot{\boldsymbol{X}}_{\mathrm{d},1}) + \boldsymbol{K}_{\mathrm{di}}(\boldsymbol{X} - \boldsymbol{X}_{\mathrm{d},1})\}, \quad (2)$$

where $\boldsymbol{X}$ denotes the tip position of the end-effector, $\boldsymbol{J}$ denotes the Jacobian matrix of the manipulator, and $\boldsymbol{D}_{\mathrm{di}}$ and $\boldsymbol{K}_{\mathrm{di}}$ denote the desired viscosity and stiffness matrices, respectively. Here, the design parameters are the nominal desired admittance and nominal desired impedance ($\boldsymbol{M}_{\mathrm{da},1}, \boldsymbol{D}_{\mathrm{da},1}, \boldsymbol{K}_{\mathrm{da},1}$, $\boldsymbol{D}_{\mathrm{di}}$, and $\boldsymbol{K}_{\mathrm{di}}$), which are individually designed in the end-effector space. In series admittance-impedance control, both accurate position tracking performance and safe contact with unknown environments can be achieved by setting the parameters to make the desired impedance hard and the desired admittance soft [2].

The equation of virtual dynamics for the 3rd layer is given as follows:

$$\begin{aligned}\boldsymbol{M}_{\mathrm{da},2}\ddot{\boldsymbol{X}}_{\mathrm{d},2} + \boldsymbol{D}_{\mathrm{da},2}\dot{\boldsymbol{X}}_{\mathrm{d},2} + \boldsymbol{K}_{\mathrm{da},2}(\boldsymbol{X}_{\mathrm{d},2} - \boldsymbol{X}_0) \\ = \int \boldsymbol{k}_{\mathrm{i}}[\boldsymbol{F}_{\mathrm{ext}}(t-T) - \boldsymbol{F}_{\mathrm{d}}]\mathrm{d}t,\end{aligned} \quad (3)$$

where $\boldsymbol{X}_0$ denotes the target position; $\boldsymbol{X}_{\mathrm{d},2}$ denotes the position of the virtual object; and $\boldsymbol{M}_{\mathrm{da},2}$, $\boldsymbol{D}_{\mathrm{da},2}$, and $\boldsymbol{K}_{\mathrm{da},2}$ denote the desired nominal inertia, viscosity, and stiffness matrices, respectively, and $\boldsymbol{F}_{\mathrm{d}}$ denotes the desired force, and $\boldsymbol{k}_{\mathrm{i}}$ denotes the integral gain. In MVDC, when generating the desired position, velocity, and acceleration for the next layer by considering the dynamics of the virtual object, as shown in (3), not only the actual force but also the virtual force computed from sensor outputs can be used. In detail, the integral of the error between the desired and actual force is used as a virtual force in the 3rd layer of the proposed method.

III. PARAMETER DESIGN FOR STABILITY IMPROVEMENT AGAINST FORCE SENSOR DELAY

This section discusses the direction of parameter design aimed at improving stability against the time delay of force sensors. In general force control methods such as admittance control and impedance control, it has been proven that increasing the damping improves stability against force sensor time delays. In MVDFC as well, since there remains design flexibility in the parameters, it is considered possible to address the issue of sensor time delay by appropriately setting the parameters. This section shows through simulation and real-world experiments that increasing the damping in the virtual dynamics improves stability against force sensor time delay.

A. Two-Dimensional Model and Parameter for Simulation

We conducted simulations on a two-dimensional plane using the 2-DOF manipulator model shown in Fig. 2 to demonstrate the improved stability against force sensor time delay by setting parameters properly. The range of motion of the manipulator is planar, and the coordinates of the end-effector are represented as $\boldsymbol{X} = [x, z]^\top$ in the fixed coordinate system $\sum_0$. The equation of motion of the two-dimensional manipulator model when the end-effector contacts the environment is given as follows:

$$\boldsymbol{M}_{\mathrm{q}}\ddot{\boldsymbol{q}} + \boldsymbol{h}_{\mathrm{q}} = \boldsymbol{\tau} - \boldsymbol{J}^\top\boldsymbol{F}_{\mathbf{ext}}, \quad (4)$$

where $\boldsymbol{q} = [q_1 \quad q_2]^\top$ denotes the angle of each joint of the manipulator, $\boldsymbol{M}_{\mathbf{q}}$ denotes the inertia matrix of the manipulator, $\boldsymbol{h}_{\mathbf{q}}$ denotes a nonlinear term including gravity and the coriolis force, $\boldsymbol{J}$ denotes the Jacobian matrix when the end-effector contacts the environment, and $\boldsymbol{\tau}$ denotes the input torque applied to each joint. Since the task involves contact with the environment, contact constraints must be considered in the simulations. We model the contact environment as a linear spring system with stiffness $K_{\mathrm{z}} = 50000$ N/m which represents hard environment because force control tends to become unstable when contacting with stiff environments in general.

The range of motion of the manipulator is planar, so the mechanical properties of the manipulator must be designed in 2D according to the desired task. Each parameter of the 2nd and 3rd virtual dynamics layers is given as follows:

$$\begin{aligned}\boldsymbol{M}_{\mathrm{da},1} &= \boldsymbol{M}_{\mathrm{da},2} = \mathrm{diag}(1.0,\ 1.0), \\ \boldsymbol{F}_{\mathrm{d}} &= \begin{bmatrix}F_{\mathrm{d,x}} & F_{\mathrm{d,z}}\end{bmatrix}^{\mathrm{T}}, \boldsymbol{k}_{\mathrm{i}} = \begin{bmatrix}k_{\mathrm{i,x}} & k_{\mathrm{i,z}}\end{bmatrix}^{\mathrm{T}}, \\ \boldsymbol{K}_{\mathrm{da},1} &= \boldsymbol{K}_{\mathrm{da},2} = \mathrm{diag}(K_{\mathrm{da},11},\ K_{\mathrm{da},22}) \\ &= \mathrm{diag}(500,\ 500).\end{aligned} \quad (5)$$

Impedance layer parameter is given as follows:

$$\begin{aligned}\boldsymbol{K}_{\mathrm{di}} &= \mathrm{diag}(K_{\mathrm{di},11},\ K_{\mathrm{di},22}) = \mathrm{diag}(5000,\ 5000), \\ \boldsymbol{D}_{\mathrm{di}} &= \mathrm{diag}(2\sqrt{K_{\mathrm{di},11}},\ 2\sqrt{K_{\mathrm{di},22}}).\end{aligned} \quad (6)$$

As shown in (5) and (6), the stiffness of impedance control is ten times greater than that of admittance control, prioritizing high-precision trajectory tracking. In this simulation, the desired contact force is achieved by switching the integral gain $\boldsymbol{k}_{\mathrm{i}}$ in (3) from 0 to the specified value after contact. The desired force is set to $F_{\mathrm{d,x}} = 0$ N and $F_{\mathrm{d,z}} = 10$ N, and the integral gain is set to $k_{\mathrm{i,x}} = 0$ and $k_{\mathrm{i,z}} = 20$. To simplify the evaluation, the joint friction and the friction between the end-effector and the environment during contact are assumed to be 0, with no noise in the feedback from the force sensor. Practical evaluation is conducted using a real manipulator in Sections III-C, D.

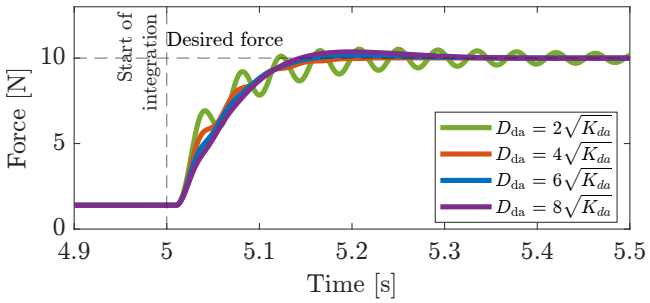

Fig. 3. Comparisons of force response in achieving desired contact force with four different viscosity.

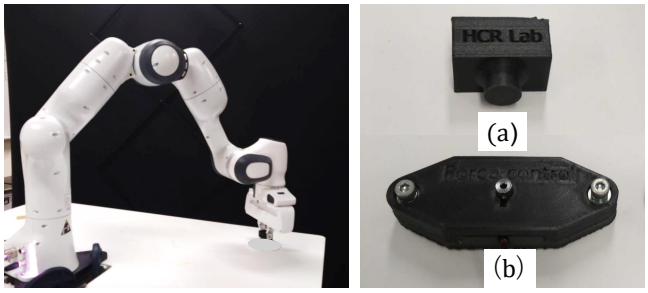

Fig. 4. Pictures of the experimental machine and environment. (a) is attached to the tip of the end-effector, and (b) is attached to the contact area. The contact experiment is conducted by pressing the tip of (a) against the metal part of (b).

B. Simulation for stability improvement against force sensor delay

First, to investigate the effect of parameter design in the virtual dynamics on stability against the force sensor time delay, a simulation was conducted by varying the parameters under a fixed time delay. The parameters include stiffness and damping; however, in this simulation, the stiffness is kept constant and only the damping value $\boldsymbol{D}_{\mathrm{da}}$ is varied, in order to conduct the investigation under a parameter setting that satisfies both high-precision trajectory tracking and safe contact. In the following, ζ denotes the damping ratio, which is assumed to be identical for both axes. The damping values in the virtual dynamics are given as follows:

$$\begin{aligned}\boldsymbol{D}_{\mathrm{da},1} = \boldsymbol{D}_{\mathrm{da},2} = \mathrm{diag}(2\zeta\sqrt{K_{\mathrm{da},11}},\ 2\zeta\sqrt{K_{\mathrm{da},22}}) \\ \zeta \in \{1, 2, 3, 4\}.\end{aligned} \tag{7}$$

The damping ratio in virtual dynamics is set in the range of 1 to 4 to investigate the relationship between the damping value and stability against the time delay of the force sensor. In addition, the dead time T of the force sensor is set to 0.01 s, considering that the actual delay in the experimental setup described in Section III-C, D is estimated to be around 0.01 s.

The simulation result when achieving desired force is shown in Fig. 3. When the damping value is set to $\boldsymbol{D}_{\mathrm{da}} = 2\sqrt{\boldsymbol{K}_{\mathrm{da}}}$, oscillations were observed due to the time delay of the force sensor. On the other hand, it was confirmed that the oscillations decreased as the damping value increased, and when $\boldsymbol{D}_{\mathrm{da}} = 6\sqrt{\boldsymbol{K}_{\mathrm{da}}}$ and $\boldsymbol{D}_{\mathrm{da}} = 8\sqrt{\boldsymbol{K}_{\mathrm{da}}}$, almost no oscillations were observed. Therefore, it can be concluded that increasing the damping value in virtual dynamics improves stability in the presence of force sensor time delay. In general, increasing the damping value is expected to reduce response speed and lead to a longer settling time. Interestingly, in contrast, the simulation results showed that even when the damping value was increased by four times, the settling time remained nearly the same, while stability against the force sensor time delay is improved. In practice, since the damping value cannot be increased indefinitely, it is necessary to choose an appropriate damping value depending on the length of time delay. As shown in Fig. 3, increasing the damping value has little downside, so it is considered reasonable to set the damping value conservatively on the higher side.

C. Experimental setup

The improvement in stability against force sensor time delay through increased viscosity in MVDFC has been demonstrated through numerical simulations. However, the conditions in actual environments are more complex, and the robustness to friction, and noise in force sensors has not yet been discussed. In this study, experiments were conducted on a two-dimensional plane using the manipulator (Franka Emika, Panda) shown on the left side of Fig. 4. This manipulator is a redundant manipulator with 7 joints for 6-DOF at the end-effector. The tip of the end-effector that comes into contact with the environment was equipped with a fixture created using a PLA filament with a 3D printer, as shown in Fig. 4(a). In contrast, the environment was constructed with an aluminum frame as a base, with the metal components in Fig. 4(b) attached to the contact area. The external force measurements of the *Franka Control Interface* (FCI) of the robot system were used for feedback and evaluation. The force was estimated using the values of the torque sensors attached to each joint of the manipulator. Regarding the sensor delay, the external force data used in the experiment are based on a torque sensor with a proprietary filter specific to the manipulator, and phase lag is introduced between the actual real-time force and estimated force [16]. The control program was developed in C++, and the control cycle was set to 0.001 s. Each parameter of admittance control and impedance control is essentially the same as those in (5) and (6), but the stiffness of impedance control is set to the value represented by the following equation:

$$\boldsymbol{K}_{\mathrm{di}} = \mathrm{diag}(K_{\mathrm{di},11},\ K_{\mathrm{di},22}) = \mathrm{diag}(2000,\ 2000). \tag{8}$$

As shown in (5) and (8), the stiffness of impedance control is four times greater than that of admittance control. The desired force is set to $F_{\mathrm{d,x}} = 0$ N and $F_{\mathrm{d,z}} = 10$ N, and integral gain is set to $k_{\mathrm{i,x}} = 0$ and $k_{\mathrm{i,z}} = 10$.

D. Experiment for stability improvement against force sensor delay

In the experiment, as in the simulation, the desired contact force is achieved by switching the integral gain $\boldsymbol{k}_{\mathrm{i}}$ in (3)

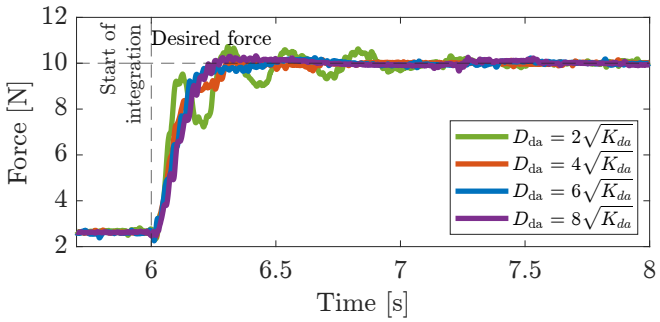

Fig. 5. Comparison of the force responses for four different viscosity.

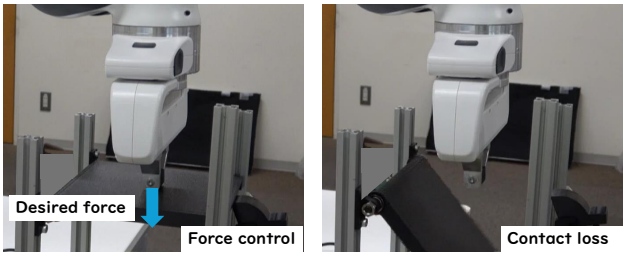

Fig. 6. Pictures of the experimental setup for contact loss with the environment.

from 0 to the specified value after contact. The viscosity in the virtual dynamics layer is the same as in (9), and the force response under four viscosity are compared. The results of force response with four different viscosity values are shown in Fig. 5. As in the simulation, when the damping was low (e.g., $\boldsymbol{D}_{\mathrm{da}} = 2\sqrt{\boldsymbol{K}_{\mathrm{da}}}$), oscillations occurred due to the time delay of the force sensor. However, the oscillations were significantly reduced as the damping increased, and were almost eliminated at $\boldsymbol{D}_{\mathrm{da}} = 6\sqrt{\boldsymbol{K}_{\mathrm{da}}}$ or $8\sqrt{\boldsymbol{K}_{\mathrm{da}}}$. Therefore, it can be concluded that increasing the damping value in virtual dynamics also improves stability against force sensor time delay also in real-world experiments. In general, increasing the damping value in the input to the robot may lead to instability in the control system due to discretization noise in velocity feedback. In contrast, in the case of MVDFC, the damping value is defined within the virtual dynamics, allowing stable control against sensor time delays without causing such instability. In addition, increasing the damping value did not significantly affect the settling time as in the simulation.

IV. PARAMETER DESIGN FOR MOTION CONTROL AFTER CONTACT LOSS

A. Utilization of Parameters in Each Layer of MVDC

This section discusses the direction of parameter design aimed at robot motion control after loss of contact with the environment. At the moment of contact loss, the external force $\boldsymbol{F}_{\mathrm{ext}}$ applied to the robot's end-effector becomes 0 instantaneously. However, the robot continues to apply force in the force control direction, causing the integral term of the virtual force in (3) to become infinitely large, which results in acceleration in the force control direction. To prevent this acceleration, it is necessary to reset the integral term to 0, in which case the virtual force in (3) also becomes 0. The behavior of the virtual object after the virtual force becomes 0 is determined by the parameters of each virtual dynamics. In addition, each virtual dynamics includes terms for the relative position, velocity, and acceleration between virtual objects. Therefore, the motion of the virtual object in the 3rd-layer virtual dynamics (3) affects that in the 2nd-layer virtual dynamics (1), which in turn influences the actual motion of the robot. Therefore, by appropriately setting the parameters of each virtual dynamics, it becomes possible to control the robot's motion after contact loss. This study focuses on viscosity among the various parameters. By designing the viscosity separately for each virtual dynamics, the convergence speed of the virtual object after the virtual force becomes 0 can be adjusted. The robot can be controlled to move in the direction opposite to that of the environment or the object upon contact loss, thereby avoiding collisions by leveraging this property.

B. Experiment of robot motion when contact is lost

We compare the robot's motion after contact loss in two cases: when the viscosity values are set separately for each virtual dynamics and when they are set equally. The experimental setup and parameters other than the viscosity values are the same as those described in Section III-C. The viscosity values are shown as follows:

$$\begin{aligned} \boldsymbol{D}_{\mathrm{da},2} &= \mathrm{diag}(2\zeta_2\sqrt{K_{\mathrm{da},11}},\ 2\zeta_2\sqrt{K_{\mathrm{da},22}}), \zeta_2 \in \{1, 4\}, \\ \boldsymbol{D}_{\mathrm{da},1} &= \mathrm{diag}(2\zeta_1\sqrt{K_{\mathrm{da},11}},\ 2\zeta_1\sqrt{K_{\mathrm{da},22}}), \zeta_1 = 4, \end{aligned} \tag{9}$$

where ζ_1, ζ_2 are damping ratio of 2nd and 3rd layer of virtual dynamics. The damping value $\boldsymbol{D}_{\mathrm{da},1}$ is set high to ensure stable control even in the presence of force sensor time delay based on the results in Section III. The damping value $\boldsymbol{D}_{\mathrm{da},2}$ is set at two different values based on this reference value. The experiment is conducted by removing the contact surface while the desired contact force is being achieved to the environment, as illustrated in Fig. 6. The results of the end-effector position and virtual object position when the contact is lost are shown in Fig. 7 and Fig. 8, where the damping ratio $\zeta_2 = 4$ and $\zeta_2 = 1$ are set for the 3rd-layer virtual dynamics, respectively.

From the graph when $\zeta_2 = 4$, after contact is lost at 1 s, the virtual object positions $z_{\mathrm{da},1}$ and $z_{\mathrm{da},2}$ exhibit an overdamped response of free vibration and gradually approach the desired position z_0. In the case of $\zeta_2 = 4$, since the 2nd and 3rd layers are configured with identical parameters, the two layers equations can be combined and regarded as a single virtual dynamics system with two virtual forces on the right side. After the contact is lost, both virtual forces become 0, resulting in a critically damped response of free vibration. However, after the contact is lost, the end-effector position z exhibits a slight movement toward the object until $z_{\mathrm{da},1}$, the equilibrium point of the first-layer impedance control, converges. This indicates a potential risk of collision with the environment.

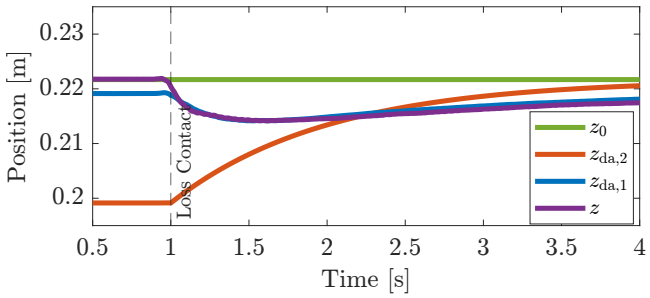

Fig. 7. Positions of the end-effector and virtual object when contact loss in the damping ratio $\zeta_2 = 4$. The damping ratio is same in the 2nd and 3rd layer of virtual dynamics.

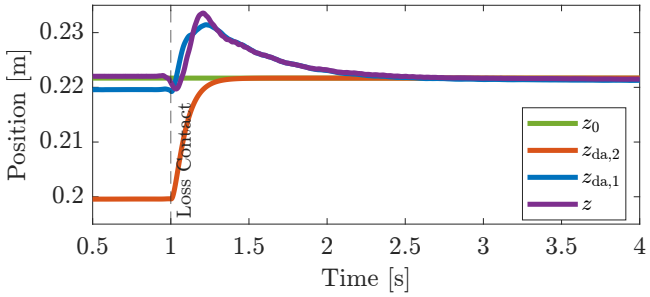

Fig. 8. Positions of the end-effector and virtual object when contact loss in the damping ratio $\zeta_2 = 1$. The damping ratio is different in the 2nd and 3rd layer of virtual dynamics.

From the graph when $\zeta_2 = 1$, after contact is lost at 1 s, the virtual object positions $z_{\mathrm{da},2}$ exhibits an critical damping response of free vibration and converge to the desired position z_0. When $\zeta_2 = 1$, the 2nd and 3rd layers have different parameter settings. As a result, the virtual object position $z_{\mathrm{da},1}$ is affected by the convergence of $z_{\mathrm{da},2}$ to the desired value, causing it to move $z_{\mathrm{da},1}$ in the direction opposite to the object, and subsequently exhibit an overdamped response. It was also confirmed that the end-effector position z instantaneously moved in the opposite direction of the object after contact loss, following $z_{\mathrm{da},1}$, and exhibited free vibration. From these results, it was verified that by designing the damping ratio of the 3rd-layer virtual dynamics to be smaller ($\zeta_2 = 1$) compared to that of the 2nd-layer virtual dynamics ($\zeta_1 = 4$), the robot's motion after contact loss can be controlled in a direction that avoids collision with the environment without controller switching. In general, robots are brought to an emergency stop upon contact loss for safety reasons. However, restarting the system and resuming the task afterward can be time-consuming. In contrast, in the proposed method, the virtual force in equation (1) becomes 0 after contact loss, resulting in the controller equation being the same before and after contact loss. Therefore, it is possible to promptly resume the task without restarting the robot.

V. CONCLUSIONS

In this research, by taking advantages of the characteristics of MVDFC; the flexibility to freely design the motion of virtual objects in each virtual dynamics independently, we propose a direction of parameter design aimed at addressing the two general challenges. The first challenge is that the control system tends to become unstable due to the time delay of the force sensor. Through simulations and experiments, it was demonstrated that increasing the damping in the virtual dynamics can improve stability against the sensor time delay without causing instability in the control system and reducing the response speed. The second challenge is the risk of collision with the surrounding environment or the target object if contact with the environment is lost during force control. Experimental results showed that by designing the damping of the 2nd-layer virtual dynamics to be large and that of the 3rd layer to be small, the end-effector moves in the direction opposite to the environment upon contact loss, thereby exhibiting behavior that avoids collisions.

REFERENCES

[1] M. Kanekiyo, H. Arita, K. Nakashima, and K. Tahara, "Desired contact force realization in unknown environments via multiple virtual dynamics-based control framework," in *Proc. Int. Conf. Autom. Sci. Eng.*, WeDT3.1, 2025.

[2] T. Fujiki and K. Tahara, "Series admittance–impedance controller for more robust and stable extension of force control," *ROBOMECH J.*, vol. 9, no. 1, p. 23, 2022.

[3] G. Kang, H. S. Oh, J. K. Seo, U. Kim and H. R. Choi, "Variable admittance control of robot manipulators based on human intention," *IEEE/ASME Trans. Mechatronics*, vol. 24, no. 3, pp. 1023-1032, 2019.

[4] N. Hogan, "Impedance control: An approach to manipulation: Part I., part II, part III," *J. Dyn. Syst., Meas., Control*, vol. 107, pp. 1–24, Mar. 1985.

[5] R. Kikuuwe, "Torque-bounded admittance control realized by a set-valued algebraic feedback," *IEEE Trans. Rob.*, vol. 35, no. 5, pp. 1136-1149, 2019.

[6] B. Yao, Z. Zhou, L. Wang, W. Xu, Q. Liu, and A. Liu, "Sensorless and adaptive admittance control of industrial robot in physical human-robot interaction," *Robotics Comput Manuf*, vol. 51, pp. 158–168, 2018.

[7] H. Arita, H. Nakamura, T. Fujiki, K. Tahara, "Smoothly Connected Preemptive Impact Reduction and Contact Impedance Control," *IEEE Trans. Rob.*, vol. 39, no. 5, pp.3536-3548, 2023.

[8] D. A. Lawrence, "Impedance control stability properties in common implementations," *Proc. IEEE Int. Conf. Robot. Autom.*, pp. 1185-1190, 1988.

[9] S.-I. Niculescu and B. Brogliato, "Force measurement time-delays and contact instability phenomenon," *Eur. J. Control*, vol. 5, no. 2–4, pp. 279–289, 1999.

[10] Y. Nagatsu and H. Hashimoto, "Friction and noise suppression for force control system based on integration of observer and force sensor information," *ROBOMECH J.*, vol. 7, no. 1, p. 7, 2020.

[11] S. Haddadin and E. Shahriari, "Unified force-impedance control," *Int. J. Robotics Res.*, vol. 43, no. 13, pp. 2112–2141, 2024.

[12] C. Schindlbeck and S. Haddadin, "Unified passivity-based Cartesian force/impedance control for rigid and flexible joint robots via task-energy tanks," in *Proc. Int. Conf. Robot. Autom.*, pp. 440–447, 2015.

[13] T. Malm, T. Salmi, I. Marstio, and J. Montonen, "Dynamic safety system for collaboration of operators and industrial robots," *Open Eng.*, vol. 9, no. 1, pp. 61–71, 2019.

[14] M. Iskandar, C. Ott, A. Albu-Schäffer, B. Siciliano and A. Dietrich, "Hybrid force-impedance control for fast end-effector motions," *IEEE Robot. Autom. Lett.*, 2023.

[15] C. C. Beltran-Hernandez, D. Petit, I. G. Ramirez-Alpizar, T. Nishi, S. Kikuchi, T. Matsubara, and K. Harada, "Learning force control for contact-rich manipulation tasks with rigid position-controlled robots," *IEEE Robot. Autom. Lett.*, vol. 5, no. 4, pp. 5709–5716, 2020.

[16] R. A. B. Petrea, M. Bertoni and R. Oboe, "On the interaction force sensing accuracy of franka emika panda robot," *IEEE Ind. Electron. Mag*, pp. 1-6, 2021.